A Study on Kicking Motion Strategy for a Legged Robot

Masashi Nakamura
Faculty of Advanced Engineering, National Institute of Technology, Maizuru College, Kyoto, Japan
Email: a0445@g.maizuru-ct.ac.jp

Takao Muromaki
Department of Mechanical Engineering, National Institute of Technology, Maizuru College, Kyoto, Japan
Email: t.muromaki@maizuru-ct.ac.jp

Takateru Urakubo
Department of Information Science, Kobe University, Kobe, Japan
Email: t.urakubo@silver.kobe-u.ac.jp

***Abstract*—For generating a translational motion of a robot in a horizontal plane or under microgravity, it is possible to utilize an impact force between the end-effector and a surface such as a wall and the ground. In this paper, we consider a legged robot consisting of four links that pushes a certain surface to obtain a translational momentum in a horizontal plane. The motion that maximizes the momentum is searched for, under the condition that the torque consumption during it is the same, by numerical optimization. The optimization results indicate that the motion with an impact force that is caused by hitting the surface is advantageous in increasing the translational momentum.**

***Index Terms*—motion planning, differential evolution, impact force**

I. Introduction

Robots perform various tasks by acting on a target object or an environment such as the ground and walls with their end-effectors. For example, a legged robot can walk or jump by pressing its toes against the ground to achieve its locomotion. Those motions are highly dependent on the gravity, and large forces are necessary to support, accelerate or decelerate the robot in a vertical direction. For generating a vertical motion against gravity, it would be necessary to continuously push the ground for a certain duration, like a human walking or jumping [1-4].

In a horizontal plane or under microgravity, robots may achieve their locomotion by different motions that cannot be performed under gravity [5-7]. Due to recent space projects, researchers are increasingly interested in the locomotion of robots under microgravity [8-10]. It would be possible to generate an impact force between the end-effector and a surface to obtain a translational momentum of a robot. A novel way of locomotion could also be realized by choosing a robot mechanism that is specialized for microgravity. However, these possibilities have not been explored sufficiently.

Impact forces are usually reduced in motion control of robots [11,12], because they tend to cause mechanical damage. To mitigate the impact forces, several robot mechanisms have been proposed so far [13,14]. Although impact forces for the motions in a horizontal plane or under microgravity would be smaller than for a vertical motion under gravity, they can be reduced by attaching an elastic component on the end-effector that contacts with a surface.

In order to save the power consumption of a robot or increase the number of tasks that a robot can accomplish, we can choose an efficient way of motion according to the tasks [15-18]. Unlike humans and other living creatures, we can also use the robot mechanisms such as the joints that do not limit joint angles. The question then arises: what is the best way of kicking out a surface by a robot with 360 degrees rotation joints especially in a horizontal plane and under microgravity?

In this paper, we consider a four-link legged robot with 360 degrees rotation joints that pushes a surface in a horizontal plane. This corresponds to a humanoid robot pushing a wall horizontally, or a hopping robot under microgravity. We perform numerical simulations for the above mentioned two ways of motion, the motion of continuously pushing a surface and the motion of hitting it with an impact force. Under the condition that the torque consumption during operation is the same, the obtained momenta for the motions are compared to confirm the advantage of the motion with an impact force.

II. Dynamical Model of Legged Robot

A. Legged Robot

Fig. 1 shows a legged robot that was developed for experiments of jumping or pushing motion. The legged robot has four links and three joints, corresponding to the

Manuscript received July 5, 2021; revised November 1, 2021.

doi: 10.18178/ijmerr.11.3.145-150

structure of the human leg. Body 1, Body 2, Body 3, and Body 4 represent the foot, lower leg, thigh, and torso, respectively. The legged robot kicks out a wall with the tip of its Body 1 (toe).

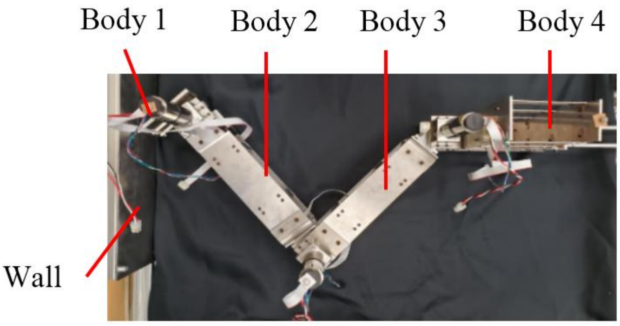

Figure 1. Legged robot

The model of contact force between the wall and the toe is important, because the translational momentum of the robot is obtained through the force. In the next subsection, we will present the equations of motion for the robot including the contact force.

B. Equation of Motion

The inertial coordinate system and the body coordinate system for each Body i are introduced as shown in Fig. 2, where l_i is the length of the body and s_i is the distance from O_i to the center of gravity G_i. The point P_i of Body i is connected to the point O_{i+1} of Body $i+1$ by a rotation joint. The equations of motion are given as follows.

$$\begin{bmatrix} \boldsymbol{M}_1 & \boldsymbol{0} & \boldsymbol{0} & \boldsymbol{0} \\ \boldsymbol{0} & \boldsymbol{M}_2 & \boldsymbol{0} & \boldsymbol{0} \\ \boldsymbol{0} & \boldsymbol{0} & \boldsymbol{M}_3 & \boldsymbol{0} \\ \boldsymbol{0} & \boldsymbol{0} & \boldsymbol{0} & \boldsymbol{M}_4 \end{bmatrix} \begin{bmatrix} \ddot{\boldsymbol{q}}_1 \\ \ddot{\boldsymbol{q}}_2 \\ \ddot{\boldsymbol{q}}_3 \\ \ddot{\boldsymbol{q}}_4 \end{bmatrix} = \begin{bmatrix} \boldsymbol{Q}_1^v \\ \boldsymbol{Q}_2^v \\ \boldsymbol{Q}_3^v \\ \boldsymbol{Q}_4^v \end{bmatrix} + \begin{bmatrix} \boldsymbol{Q}_1^c \\ \boldsymbol{Q}_2^c \\ \boldsymbol{Q}_3^c \\ \boldsymbol{Q}_4^c \end{bmatrix} + \begin{bmatrix} \boldsymbol{Q}_1^e \\ \boldsymbol{Q}_2^e \\ \boldsymbol{Q}_3^e \\ \boldsymbol{Q}_4^e \end{bmatrix}, \quad (1)$$

where $\boldsymbol{M}_i$ is an inertia matrix of Body i and is given as

$$\boldsymbol{M}_i = \begin{bmatrix} m_i & 0 & -m_i s_i \cos\phi_i \\ 0 & m_i & -m_i s_i \sin\phi_i \\ -m_i s_i \cos\phi_i & -m_i s_i \sin\phi_i & I_i + m_i s_i^2 \end{bmatrix}. \quad (2)$$

In the above equation, m_i and I_i are respectively the mass and the inertia of Body i. Its position and posture are denoted in a vector form as $\boldsymbol{q}_i = [x_i \quad y_i \quad \phi_i]^T$.

In the right-hand side of (1), $\boldsymbol{Q}_i^v$ represents the inertia force, and is given as

$$\boldsymbol{Q}_i^v = \begin{bmatrix} -m_i s_i \dot{\phi}_i^2 \sin\phi_i \\ m_i s_i \dot{\phi}_i^2 \cos\phi_i \\ 0 \end{bmatrix}. \quad (3)$$

$\boldsymbol{Q}_i^c$ represents the constraint force due to the coupling of the bodies at the joint, and is given as

$$\boldsymbol{Q}_i^c = -\left(\frac{\partial \boldsymbol{C}}{\partial \boldsymbol{q}_i}\right)^T \boldsymbol{\lambda}, \text{ where } \boldsymbol{C} = \begin{bmatrix} \boldsymbol{r}_1^P - \boldsymbol{R}_2 \\ \boldsymbol{r}_2^P - \boldsymbol{R}_3 \\ \boldsymbol{r}_3^P - \boldsymbol{R}_4 \\ y_4 \\ \phi_4 \end{bmatrix} = \boldsymbol{0}. \quad (4)$$

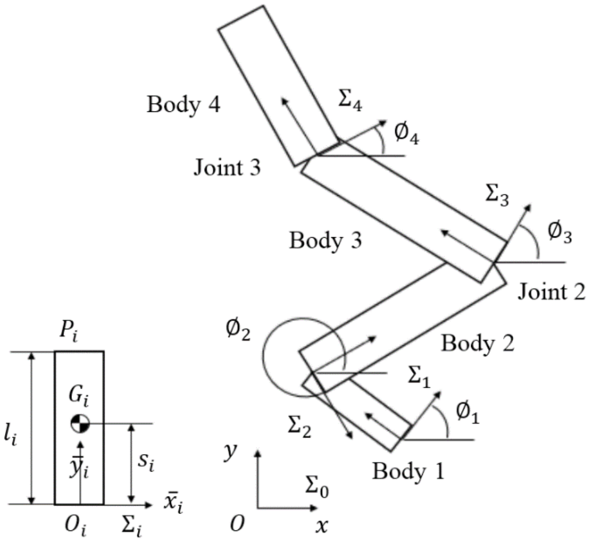

Figure 2. Body coordinate system (left) and inertial coordinate system (right).

The first three components in $\boldsymbol{C}$ express the constraints at the rotation joints, where $\boldsymbol{r}_i^P$ is the vector from O of Σ_0 to the point P_i, and $\boldsymbol{R}_i$ is a vector from O of Σ_0 to O_i of Σ_i, as shown in Fig. 3. In addition, the x-direction motion and rotational motion of Body 4 are constrained for the robot in Fig. 1, to focus only on the motion perpendicular to the wall. The last two components in $\boldsymbol{C}$ correspond to those constraints. $\boldsymbol{\lambda}$ in (4) is the vector which represents the reaction forces due to the constraints.

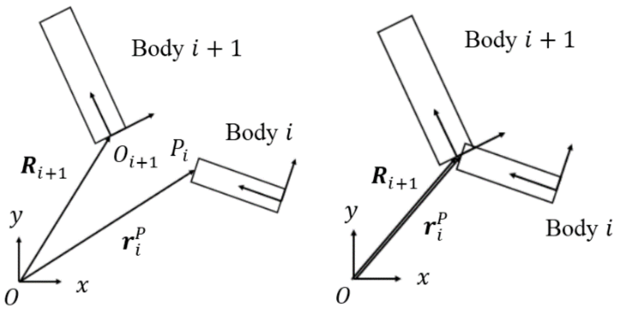

Figure 3. Constraint at the rotation joint.

The external force $\boldsymbol{Q}_i^e$ is composed of the term from the actuator torques and the term from the contact force between the toe and the wall. Let $\boldsymbol{\tau} = [\tau_1 \quad \tau_2 \quad \tau_3]^T$, where τ_i is an applied torque at Joint i. Then, the component from $\boldsymbol{\tau}$ is expressed as $\boldsymbol{H}_i \boldsymbol{\tau}$, where

$$\boldsymbol{H}_1 = \begin{bmatrix} 0 & 0 & 0 \\ 0 & 0 & 0 \\ 1 & 0 & 0 \end{bmatrix}, \boldsymbol{H}_2 = \begin{bmatrix} 0 & 0 & 0 \\ 0 & 0 & 0 \\ -1 & 1 & 0 \end{bmatrix},$$

$$\boldsymbol{H}_3 = \begin{bmatrix} 0 & 0 & 0 \\ 0 & 0 & 0 \\ 0 & -1 & 1 \end{bmatrix}, \boldsymbol{H}_4 = \begin{bmatrix} 0 & 0 & 0 \\ 0 & 0 & 0 \\ 0 & 0 & -1 \end{bmatrix}. \quad (5)$$

For $i = 2,3,4$, the external force is expressed as

$$\boldsymbol{Q}_i^e = \boldsymbol{H}_i \boldsymbol{\tau}. \quad (6)$$

For Body 1, we represent the force $\boldsymbol{Q}_1^e$ as

$$\boldsymbol{Q}_1^e = \boldsymbol{H}_1 \boldsymbol{\tau} + \boldsymbol{W}_N f_N + \boldsymbol{W}_T f_T, \quad (7)$$

$$\boldsymbol{W}_N = [0 \quad 1 \quad 0]^T, \boldsymbol{W}_T = [1 \quad 0 \quad 0]^T, \tag{8}$$

where f_N and f_T are the normal contact force and tangential force respectively. In this paper, f_N is represented by a virtual spring from the Hooke contact model [19], and f_T is expressed by a virtual damper.

$$f_N = \begin{cases} 0 & (g_N \geq 0) \\ -Kg_N & (g_N < 0) \end{cases}, \tag{9}$$

$$f_T = \begin{cases} 0 & (g_N \geq 0) \\ -\mu f_N \mathrm{sign}(\dot{g}_T) & (g_N < 0) \end{cases}, \tag{10}$$

where K is the stiffness coefficient and μ is the friction coefficient. g_N and g_T are the normal and lateral direction distances between the toe of legged robot and the wall. The normal and tangential forces act only when the toe penetrates the wall.

III. Optimization of Kicking Motion

In this paper, we search for an optimal motion of the legged robot for kicking out the wall. This section summarizes the method of calculating an optimized motion numerically.

A. Formulation of Optimization Problem

The torque $\boldsymbol{\tau}$ is assumed to be applied for $t \in [0, t_f]$, and to be kept at zero after the time t_f, as shown in Fig. 4. The legged robot gains translational momentum in the y-direction from the wall only while the toe contacts with the wall. In other words, the greater the velocity obtained when taking off the wall, the greater the movement in unit time. Therefore, we consider an optimization problem that maximizes the velocity of the center of gravity in the y-direction at the instant of taking off.

The optimization problem is formulated as follows.

$$\begin{cases} \text{Maximize} & \xi(\boldsymbol{X}) = \dot{G}_y \\ \text{w.r.t.} & \boldsymbol{X} = [\boldsymbol{\tau}^T \quad t_f \quad \emptyset_i(0)] \quad (i = 1, 2, 3) \\ \text{s.t.} & \int_0^{t_f} (\tau_1^2 + \tau_2^2 + \tau_3^2) dt = \alpha \end{cases} \tag{11}$$

Denoting the position of gravity center of the robot along y axis as G_y, evaluation function ξ is given as its time derivative after taking off. The design variable $\boldsymbol{X}$ includes the torque $\boldsymbol{\tau}$, the time t_f and the initial angles $\emptyset_i(0)$ of Body 1 to 3. Those initial angles correspond to the initial posture of the robot. It should be noted that the torque consumption for $t \in [0, t_f]$ is constrained to be the same amount of α.

Since a time history of a torque is infinite-dimensional, we express it approximately by using the Fourier series.

$$\tau_i = a_{1,i} \sin\left(\frac{\pi t}{t_f}\right) + \cdots + a_{h,i} \sin\left(\frac{h\pi t}{t_f}\right) \tag{12}$$

Then, the design variables $\tau_i(t)$ are replaced by the coefficients $a_{j,i} (i = 1, 2, 3,\ j = 1, \cdots, h)$. In addition, since it is difficult to satisfy the condition of the torques exactly, an acceptable range β is introduced.

$$\beta = ae^{-n} + b, \quad \left(a = \frac{(\rho - 1)\varepsilon}{e^{-1} - e^{-L}},\ b = \frac{e^{-1} - \rho e^{-L}}{e^{-1} - e^{-L}} \varepsilon\right), \tag{13}$$

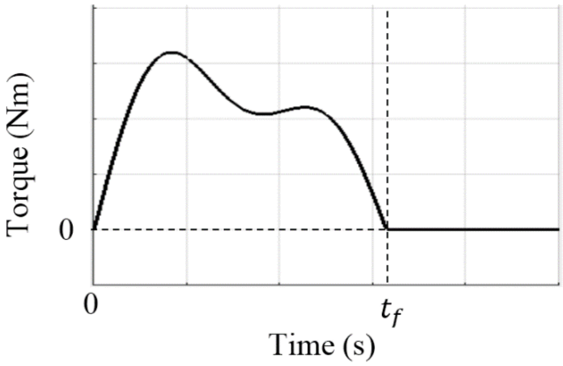

Figure 4. Example of joint torque profile.

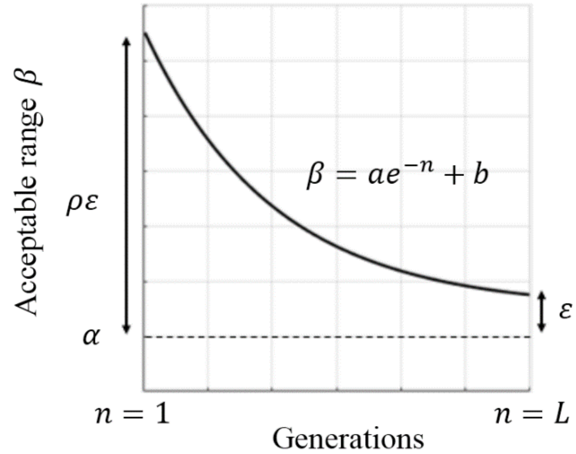

Figure 5. Acceptable range β ($\beta = \rho\varepsilon$ for $= 1$, $\beta = \varepsilon$ for $n = L$).

where n and L are the number of generations and the maximum number of generations respectively, and will be described in the next subsection. The range β is narrowed down exponentially according to n, as shown in Fig. 5, where $\rho(> 1)$ is a constant.

The evaluation function is also replaced by $\bar{\xi}(\boldsymbol{X}) = 1/\dot{G}_y$ to match the DE-based algorithm described in the next subsection. The optimization problem in (11) is rewritten as follows.

$$\begin{cases} \text{Minimize} & \bar{\xi}(\boldsymbol{X}) = 1/\dot{G}_y \\ \text{w.r.t.} & \boldsymbol{X} = [a_{j,i} \quad t_f \quad \emptyset_i(0)] \\ \text{s.t.} & J_c = \left| \int_0^{t_f} ({\tau_1}^2 + {\tau_2}^2 + {\tau_3}^2) dt - \alpha \right| \leq \beta \end{cases} \tag{14}$$

B. Algorithm Based on DE

In this paper, the optimization problem in (14) is solved with an algorithm based on Differential Evolution (DE) [20] that is described below.

(1) Generate each element of the N initial individuals $\boldsymbol{X}_k^{(1)}$ $(k = 1,2, \cdots, N)$ with a uniform random number of $[a_{min}, a_{max}]$.

(2) Repeat the following operations a) to d) with $n = 1,2, \cdots, L$, where n is called the number of generartions.

a) If the condition for the torque comsumption is satisfied, compute $\bar{\xi}(\boldsymbol{X}_k^{(n)})$ by numerical simulation. If not, set $\bar{\xi}(\boldsymbol{X}_k^{(n)}) = \infty$. Let the m-th individual $\boldsymbol{X}_m^{(n)}$ for which

$\bar{\xi}(\boldsymbol{X}_m^{(n)})$ is the smallest be the best individual $\boldsymbol{X}_{best}^{(n)}$ $(\boldsymbol{X}_{best}^{(n)} = \boldsymbol{X}_m^{(n)})$. If $\bar{\xi}(\boldsymbol{X}_k^{(n)}) = \infty$ for all $k = 1,2,\cdots,N$, the m-th individual for which J_c is the smallest is the best individual $\boldsymbol{X}_{best}^{(n)}$ $(\boldsymbol{X}_{best}^{(n)} = \boldsymbol{X}_m^{(n)})$.

b) Set the value of base vector $\boldsymbol{X}_{base}^{(n)}$ to be $\boldsymbol{X}_{best}^{(n)}$. Also, two integers $r_{1,k}$, $r_{2,k}$ $(r_{1,k} \neq r_{2,k} \neq m)$ are randomly chosen from among $k = 1,2,\cdots,N$ to generate the displacement vector $\boldsymbol{M}_k^{(n)}$ which is defined as follows.

$$\boldsymbol{M}_k^{(n)} = \boldsymbol{X}_{\mathrm{base}}^{(n)} + F\left(\boldsymbol{X}_{r_{1,k}}^{(n)} - \boldsymbol{X}_{r_{2,k}}^{(n)}\right), \tag{15}$$

where $F(> 0)$ is the scale factor.

c) Create a trial vector $\boldsymbol{U}_k^{(n)}$. Each element of $\boldsymbol{U}_k^{(n)}$, $U_{l,k}^{(n)}$ $(l = 1,2,\cdots,3h+4)$, is defined as follows.

$$U_{l,k}^{(n)} = \begin{cases} M_{l,k}^{(n)} (R_{l,k} \leq C \ \text{ or } l = l_{\mathrm{rand}}) \\ X_{l,k}^{(n)} (\text{otherwise}) \end{cases}, \tag{16}$$

where l_{rand} is a randomly chosen integer from l, $R_{l,k} \in [0\ 1]$ is a uniform random number, and $C(> 0)$ is a crossover rate.

d) Compute $\bar{\xi}(\boldsymbol{U}_k^{(n)})$. In this paper, if $\bar{\xi}(\boldsymbol{X}_k^{(n)}) \neq \infty$ or $\bar{\xi}(\boldsymbol{U}_k^{(n)}) \neq \infty$, the surviving individual is selected according to (17). If $\bar{\xi}(\boldsymbol{X}_k^{(n)}) = \infty$ and $\bar{\xi}(\boldsymbol{U}_k^{(n)}) = \infty$, it is selected according to (18).

$$\boldsymbol{X}_k^{(n+1)} = \begin{cases} \boldsymbol{U}_k^{(n)} \left(\bar{\xi}(\boldsymbol{U}_k^{(n)}) \leq \bar{\xi}(\boldsymbol{X}_k^{(n)})\right) \\ \boldsymbol{X}_k^{(n)} \left(\bar{\xi}(\boldsymbol{U}_k^{(n)}) > \bar{\xi}(\boldsymbol{X}_k^{(n)})\right) \end{cases} \tag{17}$$

$$\boldsymbol{X}_k^{(n+1)} = \begin{cases} \boldsymbol{U}_k^{(n)} \left(J_c(\boldsymbol{U}_k^{(n)}) \leq J_c(\boldsymbol{X}_k^{(n)})\right) \\ \boldsymbol{X}_k^{(n)} \left(J_c(\boldsymbol{U}_k^{(n)}) > J_c(\boldsymbol{X}_k^{(n)})\right) \end{cases} \tag{18}$$

IV. Numerical Results

A. Parameter Setting

In this section, the design variable $\boldsymbol{X}$ that minimizes $\bar{\xi}(\boldsymbol{X})$ will be obtained by the above mentioned algorithm with the following parameters; The lengths and weights of the bodies are chosen as $l_1 = 0.07$ (m), $l_2 = l_3 = 0.30$ (m), $l_4 = 0.20$ (m), $m_1 = 0.40$ (kg), $m_2 = m_3 = 1.58$ (kg), and $m_4 = 1.42$ (kg). The inertia moment of each body is calculated under the assumption that each body is a uniform bar. The coefficients K in (9) and μ in (10) are set to be $K = 170 \times 10^5$ (N/m) and $\mu = 0.1$. Considering the output of the actuators in the experimental devise, α in (11) is set to $\alpha = 0.12$. ε and ρ in (13) are chosen as $\varepsilon = 0.012$ and $\rho = 10$. The torques are represented by (12) with $h = 10$, and the range of random numbers $[a_{\min}, a_{\max}]$is set to $[-2.5, 2.5]$. The number of individuals is $N = 200$, the number of maximum generation is $L = 200$, the crossover rate is $C = 0.9$, and the scale factor is $F = 0.6$.

For numerical calculation, we make the following assumptions; a) At the initial time $t = 0$, the legged robot is stationary, and the point O_1 of Body 1 is in contact with the wall. b) The legged robot is assumed to slide on a smooth horizontal surface, and the friction between them is ignored. c) Joint friction is not considered. d) The initial angles $\phi_i(0)$ of Body 1 to 3 are constrained as follows.

$$0 \leq \phi_1(0) \leq \tfrac{\pi}{2},\ -\tfrac{\pi}{2} \leq \phi_2(0) \leq 0,\ 0 \leq \phi_3(0) \leq \tfrac{\pi}{2} \tag{19}$$

We consider two cases for numerical optimization, in order to compare two types of kicking motion: hitting the wall with an impact force and pushing the wall continuously. Although a motion such as repeatedly contacting the wall can be considered, the numerical optimization excludes it by evaluating $\dot{G}_y$ right after the toe first leaves the wall except at the initial time. To obtain the motion of pushing the wall continuously through numerical optimization, we introduce the following constraint.

$$\dot{\phi}_1 < 0 \text{ for } t > 0 \tag{20}$$

Numerical optimization was performed based on the algorithm in Sec. III in the following two cases: Case 1 without the constraint (20) and Case 2 with the constraint (20). In Case 2, we use the penalty method to find an optimized solution that satisfies the constraint (20), that is, if (20) is not satisfied, we make the evaluation function much worse.

B. Results and Discussion

The motions obtained by numerical optimization in Case 1 and Case 2 are shown in Fig. 6. The position and posture of the robot are drawn for both cases every 0.02 (s) from 0 (s) to 0.1 (s) and at 0.2 (s) in the figure, where the black dots indicate the position of the center of gravity. The torques for the motions are shown in Fig. 7, where the red, blue and green lines correspond to τ_1, τ_2, and τ_3 respectively. The time histories of normal force f_N caused at the contact point are also shown in Fig. 8.

In Case 1, the legged robot makes almost one rotation of Body 1 counterclockwise around Joint 1 as shown in Fig. 6 (a), and then hits the wall around $t = 0.087$ (s) to obtain a translational momentum through a large impact force shown in Fig. 8 (a). The velocity of center of gravity $\dot{G}_y$, that is, $\xi(\boldsymbol{X})$, is 1.544 (m/s) immediately after the toe leaves the wall at $t = 0.0874$ (s), and the height of robot G_y reaches 0.63 (m) at $t = 0.2$ (s).

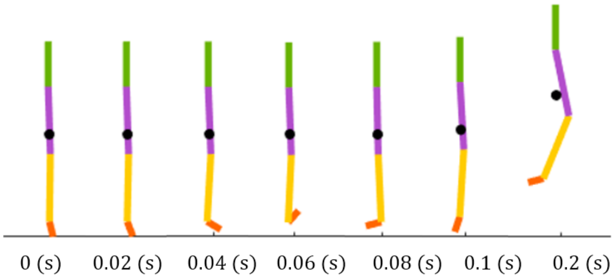

(a) Case 1

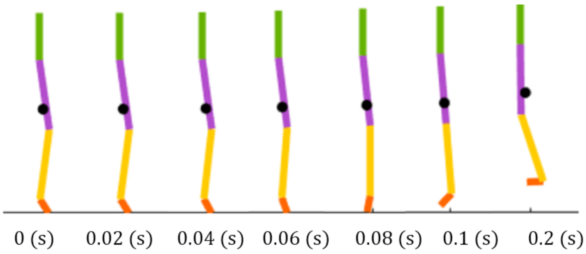

(b) Case 2

Figure 6. Position and posture obtained by numerical optimization.

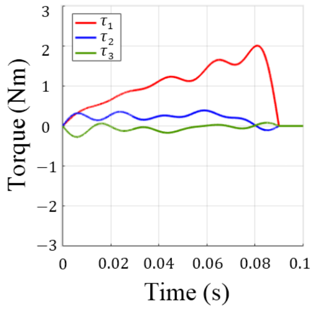

(a) Case 1

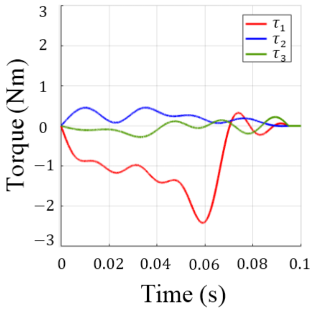

(b) Case 2

Figure 7. Joint torques for the optimized motion.

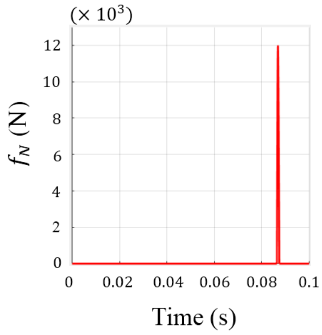

(a) Case 1

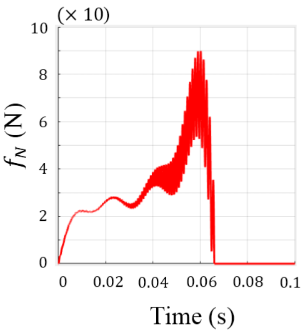

(b) Case 2

Figure 8. Normal contact force for the optimized motion.

In Case 2, the legged robot rotates Body 1 clockwise and pushes the wall continuously with the toe from the initial time, as shown in Fig. 6 (b). The contact force f_N is also caused continuously as shown in Fig. 8 (b) until the robot takes off at $t = 0.0659$ (s). The velocity of center of gravity $\dot{G}_y$, that is, $\xi(\boldsymbol{X})$, is 0.436 (m/s) after the take off, and the height of robot G_y reaches 0.51 (m) at $t = 0.2$ (s).

From these results, the velocities $\dot{G}_y$ obtained from the same amount of torque consumption are largely different in Case 1 and Case 2; the velocity in Case 1 is about 3.5 times greater than that in Case 2. It would indicate that the motion of hitting the wall with an impact force in Case 1 is advantageous in generating a large translational momentum in a horizontal plane or under microgravity.

From the time histories of joint torques in Fig. 7, almost all the allowable torque consumption is utilized to rotate Body 1 by τ_1 in both cases. In Case 1, the torque τ_1 can generate a large rotational energy of Body 1, because the toe does not contact with the wall until the hitting and the rotation of Body 1 is easily accelerated. The energy accumulated until the hitting causes a large translational momentum through the elastic collision with the wall. On the other hand, in Case 2, the rotational acceleration of Body 1 is quite reduced due to the contact force from the wall. Even though the contact force is kept applied for a longer time, the total amount of translational momentum obtained from the contact force is smaller than in Case 1. Moreover, the vibratory behavior of the contact force in Case 2 is caused from the elasticity of the contact model.

The motion of hitting a surface with an impact force would be one promising strategy for kicking in a horizontal plane or under microgravity. Although a large impact force may cause mechanical damage to the robot, the peak of the force could be mitigated by utilizing an elastic component attached on the toe. Moreover, the impact force at each joint can be estimated by $\boldsymbol{Q}_i^c$ in the dynamic model presented in Sec. II. It should be noted that the postures of robot in both cases are almost stretched out, that is, close to singular configurations. The amount of contact force that can be obtained from the energy and joint torques of robot would depend on the posture. A more detailed analysis will be performed as a future work.

V. Conclusion

In this paper, we searched for an optimal kicking motion of a legged robot in a horizontal plane by numerical optimization. The optimization results obtained by a DE-based algorithm showed that the translational momentum caused by hitting a surface with an impact force is much larger than the one by pushing it continuously, under the constraint that the torque consumption during the motion is constant. Accumulating the energy in an internal motion of the legged robot and transferring the energy to a translational momentum through a collision with a surface would be one of effective kicking motion strategies in a horizontal plane or under microgravity.

Conflict of Interest

The authors declare no conflict of interest.

Author Contributions

Masashi Nakamura conducted the research and wrote the paper; Takao Muromaki and Takateru Urakubo supervised and reviewed both research and paper; all authors had approved the final version.

Acknowledgment

This work was partially supported by JSPS KAKENHI Grant Number JP20K04350.

References

[1] B. Ugurlu and A. Kawamura, “ZMP-based online jumping pattern generation for a one-legged robot,” *IEEE Trans. on Industrial Electronics*, vol. 57, no. 5, pp. 1701-1709, May 2010.

[2] M. G. Pandy, F. E. Zajac, E. Sim, and W. S. Levine, “An optimal control model for maximum-height human jumping,” *Journal of Biomechanics*, vol. 23, no. 12, pp. 1185-1198, 1990.

[3] A. Nagano, Y. Ishige, and S. Fukashiro, “Comparison of new approaches to estimate mechanical output of individual joints in

vertical jumps," *Journal of Biomechanics*, vol. 31, issue 10, pp. 951-955, 1998.

[4] K. Miura, M. Morisawa, F. Kanehiro, S. Kajita, K. Kaneko, and K. Yokoi, "Human-like walking with toe supporting for humanoids," in *Proc. IEEE/RSJ International Conference on Intelligent Robots and Systems*, pp. 4428-4435, September 2011.

[5] S. Shimoda, T. Kubota, and I. Nakatani, "New mobility system based on elastic energy under microgravity," in *Proc. IEEE International Conference on Robotics and Automation*, vol. 3, pp. 2296-2301, 2002.

[6] A. Sayyad, B. Seth, and P. Seshu, "Single-legged hopping robotics research – A review," *Robotica*, vol. 25, pp. 587-613, 2007.

[7] K. Yoshida, "The jumping tortoise: A robot design for locomotion on micro gravity surface," in *Proc. Fifth International Symposium on Artificial Intelligence, Robotics and Automation in Space*, pp. 705-707, June 1999 (ESA SP-440).

[8] N. Rudin, H. Kolvenbach, V. Tsounis, and M. Hutter, "Cat-like jumping and landing of legged robots in low gravity using deep reinforcement learning," *IEEE Trans. on Robotics* (Early Access), June 2021.

[9] H. Kolvenbach, E. Hampp, P. Barton, R. Zenkl, and M. Hutter, "Towards jumping locomotion for quadrupted robots on the moon," in *Proc. IEEE/RSJ International Conference on Intelligent Robots and Systems*, pp. 5459-5466, November 2019.

[10] W. Brinkmann, A. Dettmann, L. C. Danter, C. Schulz, T. Stark, and A. Brandt, "Enhancement of the six-legged robot Manits for assembly and construction tasks in lunar mission scenarios within a multi-robot team," in *Proc. 15th International Symposium on Artificial Intelligence, Robotics and Automation in Space*, 5043, October. 2020.

[11] H. Gao, Y. Liu, L. Ding, G. Liu, Z. Deng, Y. Liu, and H. Yu, "Low impact force and energy consumption motion planning for hexapod robot with passive compliant ankles," *Journal of Intelligent & Robotic Systems*, no. 94, pp. 349-370, 2019.

[12] M. Luneckas, T. Luneckas, and D. Udris, "Leg placement algorithm for foot impact minimization," *International Journal of Advanced Robotic Systems*, vol. 15, pp. 1-10, 2018.

[13] J. J. Rond, M. Cardani, M. I. Campbell, and J. W. Hurst, "Mitigating peak impact forces by customizing the passive foot dynamics of legged robot," *Journal of Mechanisms and Robotics*, vol. 12, no. 5, 051010, 2020.

[14] W. Choi, C. Zhou, G. A. Medrano-Cerda, D. G. Caldwell, and N. G. Tsagarakis, "A new foot sole design for humanoids robots based on viscous air damping mechanism," in *Proc. IEEE/RSJ International Conference on Intelligent Robots and Systems*, pp. 4498-4503, 2015.

[15] T. Urakubo, T. Mashimo, and T. Kanade, "Efficient pulling motion of a two-link robot arm near singular configuration," in *Proc. IEEE/RSJ International Conference on Intelligent Robots and Systems*, pp. 1372-1377, October 2010.

[16] K. L. Brown, "Design and analysis of robots that perform dynamic tasks using internal body motion," Ph.D. Thesis, MIT, 1994.

[17] M. T. Rosenstein and R. A. Grupen, "Velocity-dependent dynamic manipulability," in *Proc. IEEE International Conference on Robotics and Automation*, vol. 3, pp. 2424–2429, 2002.

[18] C. Y. Wang, W. K. Timoszyk, and J. E. Bobrow, "Payload maximization for open chained manipulators: finding weightlifting motions for a Puma 762 robot," *IEEE Trans. on Robotics and Automation*, vol. 17, no. 2, pp. 218–224, 2001.

[19] H. Flores and H. M. Lankarani, *Contact Force Models for Multibody Dynamics*, Springer, 2016.

[20] R. Storn and K. Price, "Differential evolution-A simple and efficient heuristic for global optimization over continuous spaces," *Journal of Global Optimization*, vol. 11, pp. 341-359, 1997.

Masashi Nakamura is student in Faculty of advanced engineering at National Institute of Technology, Maizuru College, Kyoto, Japan. His research interests include dynamical modeling and numerical optimization.

Takao Muromaki received the B.E. (2006), M.E. (2008) and Ph.D. (2012) degrees in computer science and systems engineering from Kobe University, Kobe, Japan. In 2012, he joined Department of Mechanical Engineering at National Institute of Technology, Maizuru College, Maizuru, Japan, as an Assistant Professor, where he is currently an Associate Professor. His research interests include numerical optimization and systems engineering.

Takateru Urakubo received the B.E., M.E., and Ph.D. degrees in aeronautics and astronautics from Kyoto University, Kyoto, Japan, in 1996, 1998, and 2001, respectively. In 2001, he joined Kobe University, Kobe, Japan, as an Assistant Professor, where he is currently an Associate Professor with the Graduate School of System Informatics. From 2007 to 2009, he was a Visiting Research Scientist at Carnegie Mellon University, Pittsburgh, PA, USA. His current research interests include nonlinear dynamical systems, nonlinear control theory, and autonomous robots.